# Ultralow turnoff loss dual-gate SOI LIGBT with trench gate barrier and carrier stored layer*

Yi-Tao He(何逸涛), Ming Qiao(乔明)†, and Bo Zhang(张波)

*State Key Laboratory of Electronic Thin Films and Integrated Devices, University of Electronic Science and Technology of China, Chengdu* 610054, *China*

(Received 27 July 2016; revised manuscript received 25 August 2016; published online 25 October 2016)

A novel ultralow turnoff loss dual-gate silicon-on-insulator (SOI) lateral insulated gate bipolar transistor (LIGBT) is proposed. The proposed SOI LIGBT features an extra trench gate inserted between the p-well and n-drift, and an n-type carrier stored (CS) layer beneath the p-well. In the on-state, the extra trench gate acts as a barrier, which increases the carrier density at the cathode side of n-drift region, resulting in a decrease of the on-state voltage drop ($V_{on}$). In the off-state, due to the uniform carrier distribution and the assisted depletion effect induced by the extra trench gate, large number of carriers can be removed at the initial turnoff process, contributing to a low turnoff loss ($E_{off}$). Moreover, owing to the dual-gate field plates and CS layer, the carrier density beneath the p-well can greatly increase, which further improves the tradeoff between $E_{off}$ and $V_{on}$. Simulation results show that $E_{off}$ of the proposed SOI LIGBT can decrease by 77% compared with the conventional trench gate SOI LIGBT at the same $V_{on}$ of 1.1 V.

**Keywords:** lateral insulated gate bipolar transistor (LIGBT), turnoff loss, trench gate barrier, carrier stored layer

**PACS:** 73.40.Ty, 85.30.De, 85.30.Tv **DOI:** 10.1088/1674-1056/25/12/127304

## 1. Introduction

Lateral insulated gate bipolar transistor (LIGBT) based on silicon-on-insulator (SOI) substrate has been widely used in power integrated circuits (ICs) due to its advantages such as low on-state voltage drop ($V_{on}$), large current capability, and superior isolation.[1–7] However, it is well known that LIGBT suffers high turnoff loss ($E_{off}$) and slow switching owing to the removal of the large number of carriers stored in the drift region during the turnoff process. To alleviate this problem, various LIGBT structures[8–16] have been proposed, such as shorted anode LIGBT,[8] segmented anode NPN controlled LIGBT,[9,10] and gradual hole injection dual-gate LIGBT.[11] Besides, increasing the carrier density at the cathode side of the n-drift region in the on-state is an effective solution to achieve a low $E_{off}$. The typical structures are proposed in vertical or lateral IGBT,[17–23] such as injection-enhanced IGBT,[17] carrier-stored IGBT,[18,19] and dielectric barrier IGBT.[20] Based on this concept, we have proposed the SOI LIGBT with trench gate barrier (named TGB SOI LIGBT herein), which can greatly improve the tradeoff between $E_{off}$ and $V_{on}$.[23] However, the relatively lower carrier density in the region beneath the p-well limits the further reduction of device power consumption.

In this paper, a novel dual-gate SOI LIGBT with trench gate barrier (TGB) and carrier-stored (CS) layer (DTGB-CS SOI LIGBT) is proposed. A uniform carrier distribution in the n-drift region can be achieved in the on-state attributed to the TGB structure. Besides, electron injection is enhanced and carrier stored effect is realized due to the dual-gate and CS structures, respectively. The influences of device parameters on $V_{on}$ and $E_{off}$ are analyzed. Simulation results show that the DTGB-CS SOI LIGBT can achieve much better $E_{off} \sim V_{on}$ tradeoff performance than the conventional trench gate SOI LIGBT (conventional TG SOI LIGBT) and the TGB SOI LIGBT.

## 2. Device structure and mechanism

Figure 1(a) shows the schematic cross-sectional view of the proposed DTGB-CS SOI LIGBT, which features an extra trench gate (TG2) inserted between the p-well and n-drift, and an n-type carrier-stored (CS) layer beneath the p-well. Combined with the original trench gate (TG1), dual-gate structure is formed. For comparison, the schematic cross-sectional views of the TGB SOI LIGBT and conventional TG SOI LIGBT are also provided in Fig. 1(b) and Fig. 1(c), respectively. Table I shown the device parameters specification and the typical values for the three structures. Since the depth of both trench gates is the same, the DTGB-CS SOI LIGBT does not increase the manufacturing difficulty.

In the on-state, TG2 acts as a carrier barrier, which prevents the hole from injecting directly into the p-well. Therefore, the carrier density at the cathode side of the n-drift region

*Project supported by the National Natural Science Foundation of China (Grant Nos. 61376080 and 61674027) and the Natural Science Foundation of Guangdong Province, China (Grant Nos. 2014A030313736 and 2016A030311022).

†Corresponding author. E-mail: qiaoming@uestc.edu.cn

© 2016 Chinese Physical Society and IOP Publishing Ltd 

(i.e., the right side of the trench) increases and a uniform carrier distribution is realized in the n-drift region, resulting in a decrease of $V_{on}$. Due to the dual-gate field plates and CS layer, the carrier density beneath the p-well also increases greatly, which makes $V_{on}$ decrease further. In the turnoff process, large number of carriers at the cathode side are removed quickly at the voltage rise phase. Besides, the assisted depletion effect induced by TG2 can also speed up the carriers sweep-out.

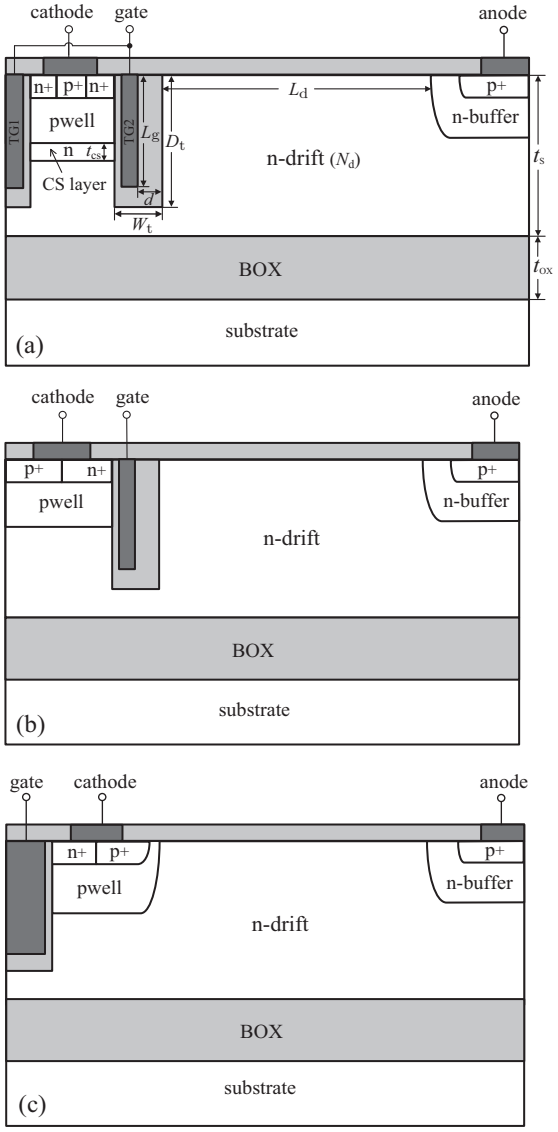



**Fig. 1.** Schematic cross-sectional views of (a) DTGB-CS SOI LIGBT, (b) TGB SOI LIGBT, and (c) conventional (conv.) TG SOI LIGBT.

**Table 1.** Device parameters specification.

| Parameters | DTGB-CS | TGB | conv. TG |
|---|---|---|---|
| SOI layer thickness, $t_s/\mu m$ | 5 | 5 | 5 |
| Buried oxide thickness, $t_{ox}/\mu m$ | 3 | 3 | 3 |
| n-drift length, $L_d/\mu m$ | 13 | 13 | 13 |
| n-drift doping, $N_d/cm^{-3}$ | $2.5 \times 10^{15}$ | $2.5 \times 10^{15}$ | $2.5 \times 10^{15}$ |
| Oxide thickness, $d/\mu m$ | 0.6 | 0.6 | – |
| Trench width, $W_t/\mu m$ | 1 | 1 | 1 |
| Trench depth, $D_t/\mu m$ | 3.5 | 3.5 | 4.5 |
| Gate length, $L_g/\mu m$ | 3.25 | 3.25 | 4.25 |
| CS layer thickness, $t_{cs}/\mu m$ | 0.5 | – | – |
| CS layer doping, $N_{cs}/cm^{-3}$ | $4 \times 10^{16}$ | – | – |

Figure 2 shows the simulated current flow lines of the three structures. For the conventional TG SOI LIGBT, holes are directly extracted from n-drift to p-well, leading to low carrier density at the cathode side of the n-drift. For the DTGB-CS and TGB SOI LIGBT, the trench gate stops the hole from injecting directly into the p-well and makes the carriers crowded at the right side of the trench. However, the carrier density in the region beneath the p-well for the TGB SOI LIGBT is still relatively low. In the DTGB-CS SOI LIGBT, the electron injection effect is enhanced and the CS effect is realized due to the dual-gate field plates and CS layer structure, which will greatly increase the carrier density in the region beneath the p-well.

Figure 3 shows the hole distributions at cutline $y = 3$ μm when $I_A = 200$ A/cm$^2$. Owing to the TGB structure, the hole density at the cathode side of the n-drift greatly increases and a uniform carrier distribution is realized. At $x = 4$ μm, the hole density of TG SOI LIGBT is below $3 \times 10^{15}$ cm$^{-3}$, while in TGB SOI LIGBT, it increases to about $3 \times 10^{16}$ cm$^{-3}$. In the DTGB-CS SOI LIGBT, the value can further increase to about $3.8 \times 10^{16}$ cm$^{-3}$. Moreover, the hole density in the region beneath the p-well also increases greatly compared with both conventional TG and TGB SOI LIGBT. Owing to the favorable uniform carrier distribution, much better tradeoff performance between $E_{off}$ and $V_{on}$ can be expected in the DTGB-CS SOI LIGBT.

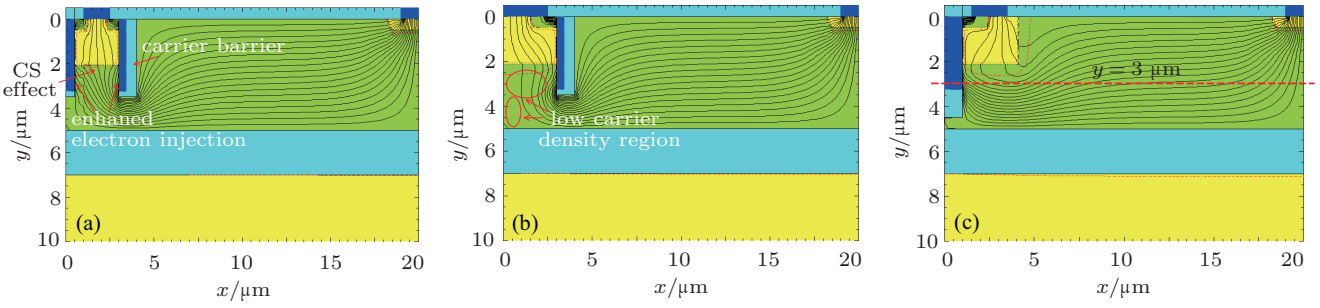



**Fig. 2.** (color online) The current flow lines of (a) DTGB-CS SOI LIGBT, (b) TGB SOI LIGBT, and (c) conventional TG SOI LIGBT at $I_A = 200$ A/cm$^2$. $I_A$ represents the anode current.

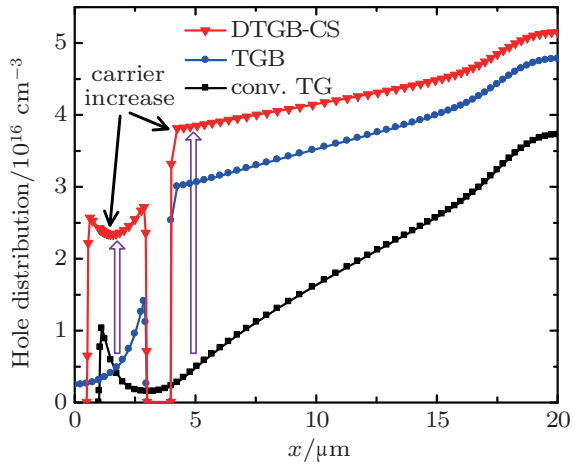



**Fig. 3.** (color online) The comparison of hole distribution for different structures at cutline $y = 3$ μm when $I_A = 200$ A/cm$^2$. The doping concentrations of p$^+$ anode are the same.

## 3. Results and discussion

The simulation is performed by two-dimensional device simulator MEDICI.[24] A lifetime of 1 μs and an ambient temperature of 300 K are used. In order to investigate the on-state and turnoff characteristics, the comparison among the DTGB-CS, TGB and conventional (conv.) TG SOI LIGBT is conducted. The typical parameter values of the three structures are shown in Table 1. At $N_d = 2.5 \times 10^{15}$ cm$^{-3}$, almost the same breakdown voltage ($BV$) can be achieved ($BV = 249$ V for conventional TG SOI LIGBT, $BV = 259$ V for DTGB-CS and TGB SOI LIGBT). $D_t$, $L_g$, and $N_{cs}$ have great influence on the $E_{off} \sim V_{on}$ tradeoff performance, and need to be discussed in the paper.

### 3.1. On-state characteristics

When the gate voltage ($V_G$) exceeds the threshold voltage and anode voltage ($V_A$) is larger than built-in voltage of the p–n junction, the device turns on and the n-drift region is under conductivity modulation. Figure 4 shows the simulated on-state $I$–$V$ curves of the different structures, in which DTGB SOI LIGBT represents the structure without CS layer. The current capability can be more than twice by introducing dual-gate structure since the channel density is doubled. For DTGB-CS SOI LIGBT, the current capability can reach as high as about 8500 A/cm$^2$ at $V_A = 20$ V. In this paper, $V_{on}$ is obtained at current density of 200 A/cm$^2$. Figure 4(b) shows that $V_{on}$ of the DTGB-CS SOI LIGBT decreases from 1.49 V for the conventional TG SOI LIGBT to only 1.05 V. This is because the carrier density at the cathode side of n-drift and in the region beneath the p-well greatly increases due to the TGB and CS layer structure, which enhances the conductivity modulation effect as shown in Fig. 3.

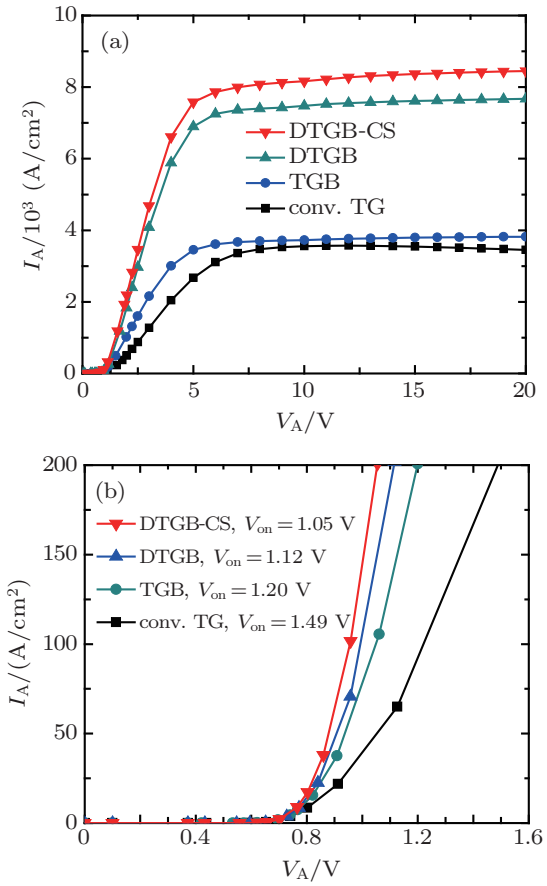



**Fig. 4.** (color online) On-state $I$–$V$ curves of different structures: (a) $V_A$ from 0 V to 20 V, and (b) $I_A$ from 0 A/cm$^2$ to 200 A/cm$^2$. For DTGB-CS, $D_t = 3.5$ μm, $L_g = 3.25$ μm and $N_{cs} = 4 \times 10^{16}$ cm$^{-3}$. For TGB, $D_t = 3.5$ μm and $L_g = 3.25$ μm. For conventional TG, $D_t = 4.5$ μm and $L_g = 4.25$ μm.

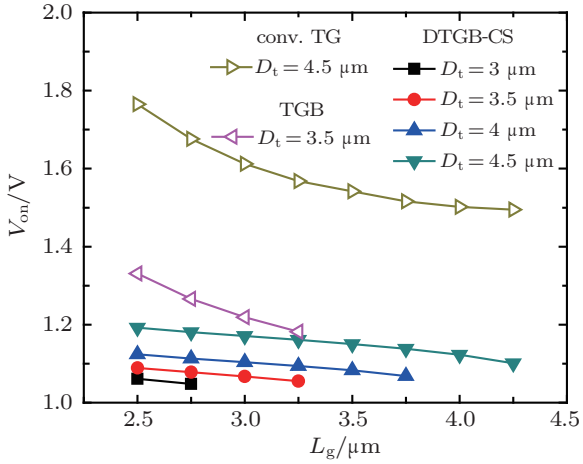



**Fig. 5.** (color online) $V_{on}$ as a function of $L_g$ for different structures.

Figure 5 shows $V_{on}$ as a function of $L_g$ for different structures when the doping concentrations of p$^+$ anode are the same. For conventional TG and TGB SOI LIGBT, $D_t$ are set as the optimal value 4.5 μm and 3.5 μm, respectively. For DTGB-CS SOI LIGBT, different $D_t$ are discussed. The DTGB-CS SOI LIGBT has lower $V_{on}$ compared with the conventional TG and TGB SOI LIGBT. At fixed $L_g$, $V_{on}$ decreases with the decrease of $D_t$ because the carriers' conductive path

becomes shorter. For each structure, with the increase of $L_g$, $V_{on}$ decreases due to the stronger electron injection from the channel inversion layer. The lowest $V_{on}$ of the conventional TG SOI LIGBT is 1.49 V when $L_g = 4.25$ μm. However, with the same $L_g$ and $D_t$, $V_{on}$ of the DTGB-CS SOI LIGBT is only 1.10 V. Also, $V_{on}$ of the DTGB-CS SOI LIGBT can decrease to 1.05 V when $D_t = 3.5$ μm and $L_g = 3.25$ μm, which is 30% lower than that of the conventional TG SOI LIGBT.

### 3.2. Turnoff characteristics

In the turnoff simulation, the device is turned off under an on-state current density of 200 A/cm$^2$ and a supply voltage of 100 V. The load inductance is 2 μH and gate resistance is 1 Ω. In order to make a fair comparison of $E_{off}$, $V_{on}$ is adjusted to the same as 1.1 V by changing the doping concentration of p$^+$ anode. Figure 6 shows the $E_{off}$ as a function of $L_g$ for DTGB-CS SOI LIGBT with different $D_t$. $E_{off}$ decreases as $L_g$ increases because larger $L_g$ can not only enhance the electron injection in the on-state but also assist the depletion of n-drift region during turnoff. Besides, $E_{off}$ will decrease as $D_t$ decreases for a shorter conductive path of carriers. When $D_t = 3.5$ μm and $L_g = 3.25$ μm, the DTGB-CS SOI LIGBT can achieve the lowest $E_{off}$ of 0.36 mJ/cm$^2$. Figure 6 also shows the $E_{off}$ as a function of $N_{cs}$, among which $N_{cs} = N_d = 2.5 \times 10^{15}$ cm$^{-3}$ means the structure without CS layer (i.e., DTGB SOI LIGBT). The $BV$ remains the same when $N_{cs}$ varies from $2.5 \times 10^{15}$ cm$^{-3}$ to $1 \times 10^{17}$ cm$^{-3}$. With the increase of $N_{cs}$, $E_{off}$ decreases for the stronger CS effects. However, $E_{off}$ will no longer decrease when $N_{cs}$ increases to above $4 \times 10^{16}$ cm$^{-3}$ since too large an $N_{cs}$ will make a longer voltage rise phase. In this paper, the optimal values are chosen as $D_t = 3.5$ μm, $L_g = 3.25$ μm and $N_{cs} = 4 \times 10^{16}$ cm$^{-3}$.

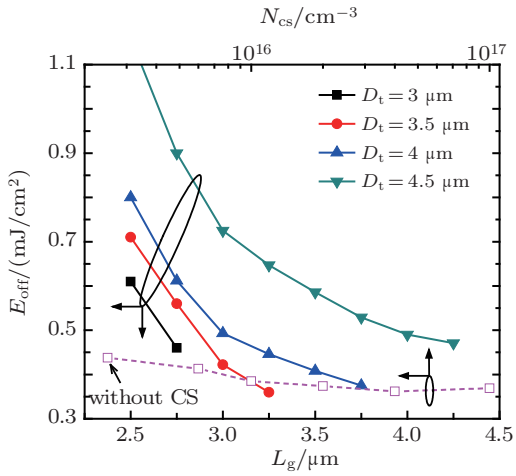



**Fig. 6.** (color online) $E_{off}$ as a function of $L_g$ ($N_{cs} = 4 \times 10^{16}$ cm$^{-3}$) and $N_{cs}$ ($L_g = 3.25$ μm, $D_t = 3.5$ μm) for the DTGB-CS SOI LIGBT. All the $E_{off}$ is obtained at $V_{on} = 1.1$ V

Figure 7 shows the inductive turnoff waveforms of DTGB-CS SOI LIGBT with different $L_g$, $D_t$, and $N_{cs}$ at $V_{on} = 1.1$ V. With the increase of $L_g$, the electron injection is enhanced and the carrier density at the anode side of the n-drift is decreased at the same $V_{on}$, which makes the current fall time decrease as shown in Fig. 7(a). However, the current delay time increases as $L_g$ increases since the gate-drain capacitance ($C_{gd}$) increases. Figure 7(b) shows that as $D_t$ increases, both the current fall time and the current delay time greatly increase. That is because more carriers are stored in the n-drift region due to the longer conductive path of carriers. Figure 7(c) compares the turnoff waveforms between DTGB SOI LIGBT (i.e. $N_{cs} = 2.5 \times 10^{15}$ cm$^{-3}$) and DTGB-CS SOI LIGBT with $N_{cs} = 4 \times 10^{16}$ cm$^{-3}$. Although the current delay time increases by adding the CS layer, a smaller current fall time can be achieved in the DTGB-CS SOI LIGBT, leading to a lower $E_{off}$.

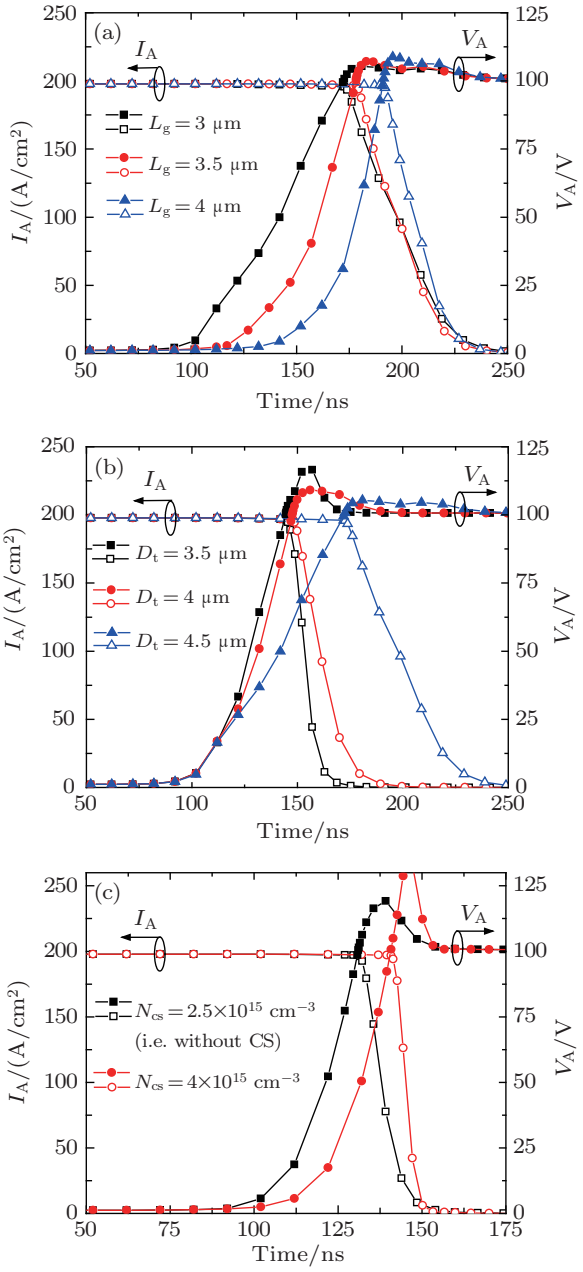



**Fig. 7.** (color online) Inductive turnoff waveforms of the DTGB-CS SOI LIGBT with (a) different $L_g$ ($D_t = 4.5$ μm, $N_{cs} = 4 \times 10^{16}$ cm$^{-3}$), (b) different $D_t$ ($L_g = 3$ μm, $N_{cs} = 4 \times 10^{16}$ cm$^{-3}$), and (c) different $N_{cs}$ ($L_g = 3.25$ μm, $D_t = 3.5$ cm$^{-3}$).

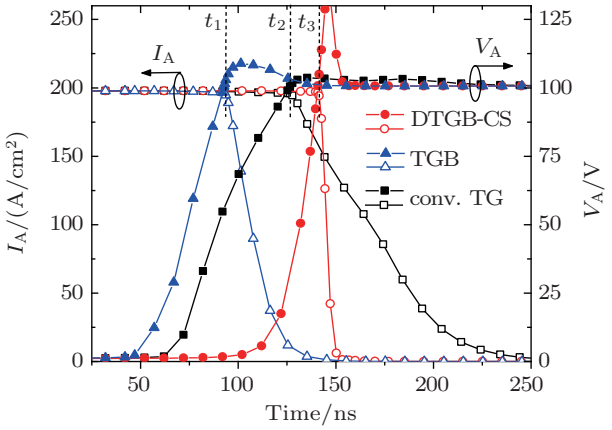



**Fig. 8.** (color online) Inductive turnoff waveforms of the DTGB-CS, TGB and conventional TG SOI LIGBT when $V_{on} = 1.1$ V. All devices are optimally designed (DTGB-CS: $D_t = 3.5$ μm, $L_g = 3.25$ μm and $N_{cs} = 4 \times 10^{16}$ cm$^{-3}$; TGB: $D_t = 3.5$ μm and $L_g = 3.25$ μm; conventional TG: $D_t = 4.5$ μm and $L_g = 4.25$ μm).

Based on the discussion above, the optimal parameters of the DTGB-CS SOI LIGBT can be obtained as follows: $D_t = 3.5$ μm, $L_g = 3.25$ μm and $N_{cs} = 4 \times 10^{16}$ cm$^{-3}$. Figure 8 shows the inductive turnoff waveforms of the optimized three structures when $V_{on} = 1.1$ V. The current delay time of the DTGB-CS SOI LIGBT ($t_3$) is the longest since the $C_{gd}$ is increased due to the dual-gate structure. However, the DTGB-CS SOI LIGBT can achieve the smallest current fall time. The current fall times of the DTGB-CS, TGB and conventional TG SOI LIGBT are about 8 ns, 27 ns, and 84 ns, respectively. Therefore, the DTGB-CS SOI LIGBT performs with much lower turnoff loss.

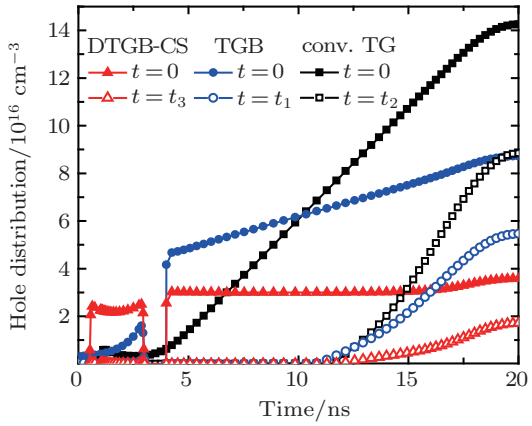



**Fig. 9.** (color online) Hole distribution at cutline $y = 3$ μm during turnoff. $t_2$, $t_1$, and $t_3$ denote the times when current begins to fall for the conventional TG, TGB, and DTGB-CS SOI LIGBT, respectively.

Figure 9 shows the hole distribution at cutline $y = 3$ μm of the three structures during turnoff process. At $t = 0$, the DTGB-CS SOI LIGBT shows the most uniform carrier distribution among the three devices at the same $V_{on} = 1.1$ V. Due to the TGB structure, the carrier density of the DTBG-CS SOI LIGBT greatly increases at $x = 4$ μm and decreases at $x = 20$ μm compared with that of the conventional TG SOI LIGBT. The carrier density in the region beneath the p-well (0.5 μm$< x <$ 3.5 μm) greatly increases to above $2 \times 10^{16}$ cm$^{-3}$ owing to the carrier stored effects, which also means the carrier density is smaller than that of the TGB SOI LIGBT at entire n-drift region ($x > 4$ μm). The favorable uniform carrier distribution of the DTGB-CS SOI LIGBT means that the overall number of carriers stored in the drift region is greatly reduced. During the initial turnoff process, larger number of carriers at the cathode side of the DTGB-CS SOI LIGBT can be quickly swept out within a small rise of $V_A$. At the end of the $V_A$ rise (i.e., the beginning of the current fall), the carrier density in the DTGB-CS SOI LIGBT is much smaller than that of the other two structures. Therefore, much smaller current fall time can be achieved.

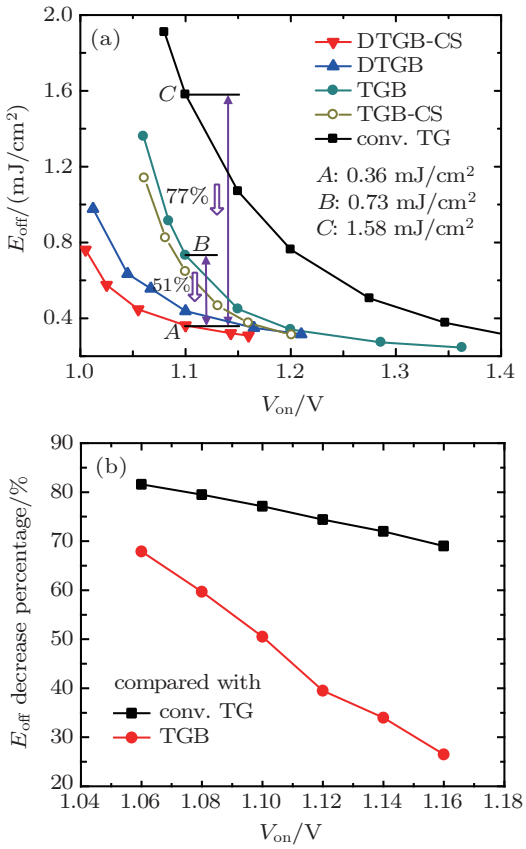



**Fig. 10.** (color online) (a) Tradeoff performances between $E_{off}$ and $V_{on}$ of different structures. (b) $E_{off}$ decrease percentage under different $V_{on}$. All the devices are optimally designed.

Figure 10(a) shows the tradeoff performances between $E_{off}$ and $V_{on}$, in which the TGB-CS SOI LIGBT represents the TGB SOI LIGBT with CS layer and all the structures are optimally designed. The DTGB-CS SOI LIGBT can realize the best tradeoff performance. At the same $V_{on}$ of 1.1 V, $E_{off}$ of the DTGB-CS SOI LIGBT (0.36 mJ/cm$^2$) can be decreased by 77% compared with that of the conventional TG SOI LIGBT (1.58 mJ/cm$^2$), and by 51% compared with that of the TGB SOI LIGBT (0.73 mJ/cm$^2$). Besides, DTGB-CS SOI LIGBT shows better performance than DTGB SOI LIGBT owing to the CS layer structure. Figure 10(b) shows the $E_{off}$ decrease percentage under different $V_{on}$. $E_{off}$ decrease percentages are

69% and 27% compared with conventional TG and TGB SOI LIGBT under $V_{on}$ of 1.16 V. However, the decrease percentages can increase to 82% and 68% when $V_{on}$ decreases to 1.06 V. Therefore, DTGB-CS SOI LIGBT has greater advantage over conventional TG and TGB SOI LIGBT under lower $V_{on}$.

## 4. Conclusion

In conclusion, a novel ultralow turnoff loss DTGB-CS SOI LIGBT is proposed. The extra trench gate acts as a barrier to prevent the hole from injecting directly into the p-well in the on-state, which increases the carrier density at the cathode side of the n-drift region, resulting in a decrease of $V_{on}$. Besides, due to the uniform carrier distribution and the assisted depletion effect induced by the extra trench gate, large number of carriers can be quickly removed at the initial turnoff process, leading to a decrease of $E_{off}$. Moreover, the carrier density beneath the p-well can greatly increase owing to the dual-gate field plates and CS layer, which further improves the trade-off between $V_{on}$ and $E_{off}$. With $D_t = 3.5$ μm, $L_g = 3.25$ μm and $N_{cs} = 4 \times 10^{16}$ cm$^{-3}$, the DTGB-CS SOI LIGBT can achieve 77% lower $E_{off}$ compared with the conventional TG SOI LIGBT, or 51% lower $E_{off}$ compared with the TGB SOI LIGBT at the same $V_{on}$ of 1.1 V.

## References


[1] Simpson M R, Gough P A, Hshieh F I and Rumennik V 1985 *Proc. IEDM*, p. 740

[2] Leung Y, Paul A, Plummer J and Wong S 1998 *IEEE Trans. Electron Dev.* **45** 2251

[3] Kho E C T, Hoelke A D, Pilkington S J, Pal D K, Abidin W A W Z, Ng L Y, Antoniou M and Udrea F 2012 *IEEE Electron Dev. Lett.* **33** 1291

[4] Nitta T, Yanagi S, Miyajima T, Furuya K, Otsu Y, Onoda H and Hatasako K 2006 *Proc. ISPSD*, June 4–8, 2006, Naples, Italy, p. 1

[5] Zhu J, Zhang L, Sun W F, Du Y C, Huang K Q, Chen M, Shi L X, Gu Y and Zhang S 2016 *IEEE Trans. Electron Dev.* **63** 1161

[6] Qiao M, Zhang K, Zhou X, Zou J, Zhang B and Li Z J 2015 *IEEE Trans. Electron Dev.* **62** 1970

[7] Qiao M, Zhou X, He Y T, Wen H J, Zhao Y Y and Zhang B 2012 *IEEE Electron Dev. Lett.* **33** 1438

[8] Chul J H, Byeon D S, Oh J K, Han M K and Choi Y I 2000 *Proc. ISPSD*, May 22–25, 2000, Toulouse, French, p. 149

[9] Hardikar S, Tadikonda R, Sweet M, Vershinin K and Narayanan E M S 2003 *IEEE Trans. Electron Dev.* **24** 701

[10] Green D W, Sweet M, Vershinin K V, Hardikar S and Narayanan E M S 2005 *IEEE Trans. Electron Dev.* **52** 2482

[11] Lee B H, Chun J H, Kim S D, Byeon D S, Lee W O, Han M K and Choi Y I 1998 *Electron Dev. Lett.* **19** 490

[12] Udugampola N K, McMahon R A, Udrea F and Amaratunga G 2005 *IEEE Trans. Electron Dev.* **52** 99

[13] Chen W S, Li Z J and Zhang B 2010 *IEEE Electron Dev. Lett.* **31** 467

[14] He Y T, Qiao M, Zhou X, Li Z J and Zhang B 2015 *IEEE Trans. Electron Dev.* **62** 3774

[15] Chen W Z, Li Z H, Zhang B, Ren M, Zhang J P, Liu Y and Li Z J 2014 *Chin. Phys. B* **23** 018505

[16] Fu Q, Zhang B, Luo X R and Li Z J 2013 *Chin. Phys. B* **22** 077309

[17] Mori M, Oyama K, Kohno Y, Sakano J, Uruno J, Ishizaka K and Kawase D 2007 *IEEE Trans. Electron Dev.* **54** 2011

[18] Takahashi H, Haruguchi H, Hagino H and Yamada T 1996 *Proc. ISPSD*, May 20–23, 1996, Maui, HI, USA, p. 349

[19] Takahashi S, Akio A, Youichi Y, Satoshi S and Norihito N 2012 *Proc. ISPSD*, June 3–7, 2012, Bruges, Belgium, p. 393

[20] Takei M, Fujikake S, Nakazawa H, Naito T, Kawashima T, Shimoyama K and Kuribayashi H 2010 *Proc. ISPSD*, June 6–10, 2010, Hiroshima, Japan, p. 383

[21] Meng H, Chen J, Frank X C J and Lin X N 2014 *Proc. ICSICT*, October 28–31, 2014, Guilin, China, p. 1

[22] Zhang J P, Li Z H, Zhang B and Li Z J 2014 *Chin. Phys. B* **23** 088504

[23] He Y T, Qiao M, Zhang B and Li Z J 2016 *Superlattices and Microstructures* **89** 179

[24] Synopsys Inc., Fremont, CA, MEDICI, Two Dimensional Device Simulation Program, 2004